

CONSTITUTIVE MODEL FOR WOOD BASED ON CONTINUUM DAMAGE MECHANICS

Carmen Sandhaas¹, Jan-Willem van de Kuilen², Hans Joachim Blass³

ABSTRACT: Based on the theory of continuum damage mechanics (CDM), a 3D constitutive model was developed that allows for a holistic approach for timber models. With one single material model, simultaneous ductile and brittle behaviour of wood can be simulated and the failure modes can be identified. To validate the model, tension, compression and embedment tests were modelled applying the developed constitutive model. Not only softwoods were used, but also European and tropical hardwoods. The predictive quality of the constitutive model was assessed by comparing load-slip curves and failure modes of the test specimens with the numerical results. Good agreements were found and brittle behaviour with stable crack growth could be predicted. The developed material model proved to be a valid approach to improve the prediction quality of numerical models and to identify failure modes.

KEYWORDS: 3D constitutive model wood, continuum damage mechanics (CDM), finite element method

1 INTRODUCTION

Wood and timber connections are difficult to model. Apart from heterogeneity, two other main material-specific issues lead to numerical problems: anisotropy with different strength in tension and compression and ductile and brittle failure modes occurring simultaneously. Within the framework of continuum damage mechanics (CDM), a general approach combining the above mentioned issues in one single 3D material model was developed. This developed constitutive model was used to predict material behaviour and embedment tests.

2 DEFINITIONS

Material directions and arrays must be clearly defined before introducing the material model. Both are given in Equation (1) and Figure 1. The known indices in timber engineering are used, e.g. index v = longitudinal shear, index 90 = direction perpendicular-to-grain.

¹ Carmen Sandhaas, Timber Structures and Wood Technology, Delft University of Technology, Stevinweg 1, 2628 CN Delft, the Netherlands. Since 1 October 2011: Institute for Timber Structures and Building Construction, Karlsruhe Institute of Technology, Germany. Email: sandhaas@kit.edu

² Jan-Willem G van de Kuilen, Holzforschung München, Technical University Munich, Winzererstrasse 45, 80797 München, Germany. Email: vandekuilen@wzw.tum.de

³ Hans Joachim Blass, Institute for Timber Structures and Building Construction, Karlsruhe Institute of Technology, R.-Baumeister-Platz 1, 76131 Karlsruhe, Germany. Email: hans.blass@kit.edu

$$\sigma = \begin{bmatrix} \sigma_{11} & \sigma_{22} & \sigma_{33} & \sigma_{12} & \sigma_{13} & \sigma_{23} \end{bmatrix}^T \triangleq \begin{bmatrix} \sigma_L & \sigma_R & \sigma_T & \sigma_{LR} & \sigma_{LT} & \sigma_{RT} \end{bmatrix}^T \triangleq \begin{bmatrix} \sigma_0 & \sigma_{90R} & \sigma_{90T} & \sigma_{vR} & \sigma_{vT} & \sigma_{roll} \end{bmatrix}^T \quad (1)$$

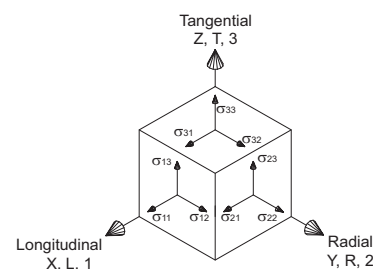


Figure 1: Definition of material direction and stress components

The developed material model is orthotropic. However, the same material properties were used for the radial and the tangential direction having thus a smeared direction perpendicular-to-grain.

3 FAILURE MODES

Classical theory of plasticity is generally based on single-surface failure criteria that are not able to identify failure modes as the material starts failing in all material directions once the failure criterion is exceeded. Examples are the wide-spread Hill [1] or Hoffman [2] criteria.

Therefore, in order to recognise failure modes, the single-surface was divided; different failure criteria were assigned to stress components that were valid only for the respective stress-strain quadrants. For

implementation this means that a case distinction has to be carried out for the single normal stress components at every increment in order to assign the single failure criteria:

- $\sigma_L \geq 0$ - Criterion I: Failure in tension parallel-to-grain is a brittle failure mode of wood which is caused by tensile stresses σ_L parallel-to-grain. It is assumed that other stress components do not influence the tension strength parallel-to-grain. Maximum stress criterion:

$$F_{t,0}(\sigma) = \frac{\sigma_L}{f_{t,0}} \leq 1 \quad (2)$$

- $\sigma_L < 0$ - Criterion II: Failure in compression parallel-to-grain is a ductile failure mode of wood which is caused by compression stresses σ_L parallel-to-grain. Maximum stress criterion:

$$F_{c,0}(\sigma) = \frac{-\sigma_L}{f_{c,0}} \leq 1 \quad (3)$$

The transverse tension modes and shear modes have to be combined as for instance splitting parallel to the LR-plane can be caused by tension perpendicular-to-grain (mode I), shear (mode II) or a combination of both (mixed mode). It is not possible to define separate failure modes for each stress component as degradation of one component also leads to degradation of the other components. This means that damage due to longitudinal shear also leads to damage in tension perpendicular-to-grain even though the actual normal tension stress component perpendicular-to-grain may still be lower than the transverse tension strength.

- $\sigma_{R/T} \geq 0$ - Criteria III / IV: Failure in tension perpendicular-to-grain with splitting in LT-plane resp. in LR-plane is a brittle failure mode of wood which is caused by tensile stresses $\sigma_{R/T}$ in the radial direction, longitudinal shear stresses $\sigma_{LR/LT}$ in the LT-plane or rolling shear stresses σ_{RT} . Quadratic criterion:

$$F_{t,90R/T}(\sigma) = \frac{\sigma_{R/T}^2}{f_{t,90}^2} + \frac{\sigma_{LT/LR}^2}{f_v^2} + \frac{\sigma_{RT}^2}{f_{roll}^2} \leq 1 \quad (4)$$

- $\sigma_{R/T} < 0$ - Criteria V - VIII: Two failure modes “pure transverse compression” and “shear”, both occurring under compression perpendicular-to-grain, are distinguished. Failure in compression perpendicular-to-grain is a ductile failure mode of wood which is caused only by compression stresses $\sigma_{R/T}$ in radial direction. Brittle shear failure can also occur if for instance the compression load is applied with an angle to the grain creating high shear stress components. Therefore, also a failure criterion for high shear stresses under simultaneous compression perpendicular-to-grain must be introduced:

$$F_{c,90R/T}(\sigma) = \frac{-\sigma_{R/T}}{f_{c,90}} \leq 1 \quad (5)$$

$$F_{vR/T}(\sigma) = \frac{\sigma_{LT/LR}^2}{f_v^2} + \frac{\sigma_{RT}^2}{f_{roll}^2} \leq 1 \quad (6)$$

4 METHODOLOGY

4.1 DAMAGE EVOLUTION

CDM is a nonlinear elastic approach where the nonlinear behaviour is obtained by modifying the stiffness matrix **D** or its inverse, the compliance matrix **C**. CDM can be implemented in an incremental-iterative FE framework. The stress increments are calculated from strain increments via a variable stiffness matrix. Therefore and as opposed to classical plasticity, the unloading in damage mechanics is following the secant stiffness and not following the elastic stiffness, see Figure 2. No plastic deformations can be modelled. CDM is a widespread approach for fibre composites modelling, many different models have already been developed, e.g. [3] or [4].

In CDM, a damage variable d , $0 \leq d \leq 1$, is determined and inserted into the fundamental Hooke equation as follows:

$$\sigma_{ij} = (1-d)D_{ijkl}\varepsilon_{kl} \quad (7)$$

If $d=0$, no damage is present; if $d=1$, the material has failed. This principle of CDM as a nonlinear elastic approach is visualised in Figure 2.

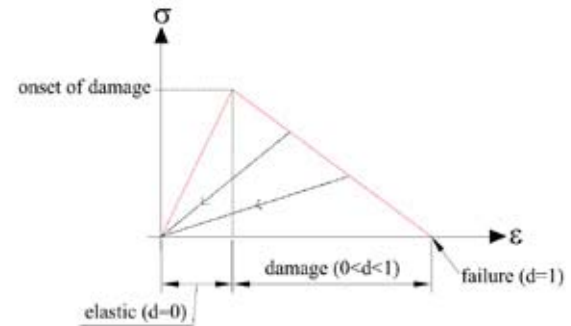


Figure 2: Basic idea of CDM, linear damage function

However, anisotropic damage is observed for wood which means that several damage variables must be defined to represent the 3D behaviour of wood. Exceeding the above described failure criteria I to VIII activated conjugated damage variables d where the shear damage variables can develop under transverse tension and compression and have to be superposed:

- Criterion I: $d_{t,0}$
- Criterion II: $d_{c,0}$
- Criteria III and IV: $d_{t,90R/T}$, $d_{vR/T}$ and d_{roll}
- Criteria V to VIII: $d_{c,90R/T}$, $d_{vR/T}$ and d_{roll}

As for instance the first two damage variables $d_{t,0}$ and $d_{c,0}$ are depending on the same stress component σ_L , the Macaulay operator as defined in Equation (8) is used to differentiate between tension and compression, Equation (9):

$$\langle a \rangle := \frac{(a + |a|)}{2} \quad (8)$$

$$d_0 = d_{t,0} \frac{\langle \sigma_L \rangle}{|\sigma_L|} + d_{c,0} \frac{\langle -\sigma_L \rangle}{|\sigma_L|} \quad (9)$$

Two different stress-strain behaviours are implemented, elastic perfectly plastic and elastic linear softening. Exceeding the compression strength triggers ductile stress-strain behaviour where the damage variable follows an elastic perfectly plastic law:

$$d(\kappa) = 1 - \frac{1}{\kappa} \quad (10)$$

The failure criteria for tension and shear instead lead to a linear softening stress-strain relationship as illustrated in Figure 2:

$$d(\kappa) = 1 - \frac{1}{f_{\max}^2 - 2G_f E} \left(f_{\max}^2 - \frac{2G_f E}{\kappa} \right) \quad (11)$$

where f_{\max} = maximum strength, E = modulus of elasticity, G_f = fracture energy.

As can be seen in Equations (10) and (11), the development of the damage variables is not depending on the strains ε , but on a history parameter κ instead. The damage parameters d cannot be a function of the strains ε . For instance, once failure criterion III ($= F_{t,90R}$, splitting parallel to LT-plane) is activated due to high longitudinal shear stresses σ_{LT} , the stiffness values of all other contributing stress components (E_R and E_{RT}) must degrade as well although the resp. uniaxial stresses σ_R and σ_{RT} may still be below the uniaxial strengths $f_{t,90}$ and f_{roll} . In such a case, a dependency of the damage parameters $d_{t,90}$ and d_{roll} on the strains ε_R and ε_{RT} may not trigger the evolution of damage in these secondary directions. A dependency on the history parameters $\kappa_{t,90}$ and κ_{roll} will enforce the evolution of the damage parameters $d_{t,90}$ and d_{roll} instead. The physical reason behind the enforcing of damage although the uniaxial strengths may not be exceeded is obvious: once a wooden piece has failed in shear parallel to the LT-plane, it will not be able to take any loads in tension perpendicular to the LT-plane.

The failure criteria F can be reformulated introducing state variables κ that keep track of the loading history:

$$\Theta(F, \kappa) = F - \kappa \leq 0 \quad (12)$$

This principle is analogous to the flow theory of plasticity. The “yield” surfaces F are the damage initiation functions or failure criteria. As in classical plasticity and following [4], the so-called Kuhn-Tucker conditions must hold:

$$\Theta \leq 0, \quad \dot{\kappa} \geq 0, \quad \kappa \dot{\Theta} = 0 \quad (13)$$

Furthermore, it is required that the damage variables can only grow as given in Equation (14) which follows also from the second Kuhn-Tucker condition.

$$\dot{d} \geq 0 \quad (14)$$

The final implementation of the history parameters as state variables is carried out as shown in Equation (15):

$$\kappa' = \max \left\{ 1, \max_{incr=0,t} \{ F^{incr} \} \right\} \quad (15)$$

4.2 CONSTITUTIVE MODEL

The introduced damage variables have to be combined in a constitutive model, Equation (16) shows the constitutive relationship between strains ε and stresses σ with C^{dam} being the damaged compliance matrix.

$$\varepsilon = C^{dam} \sigma \quad (16)$$

In this damaged compliance matrix which is the analogous formulation to Equation (7) showing the damaged stiffness matrix $(1-d) \cdot D$, damage effects and interactions have to be represented. For instance, damage in compression parallel-to-grain could be assumed to lead to a decrease of the stiffness in tension parallel-to-grain during a subsequent loading cycle. Furthermore, assumptions about the effects of damage parallel-to-grain on the strength perpendicular-to-grain need to be taken.

In the developed material model, no damage interactions were modelled. For instance, it is assumed that damage in tension perpendicular-to-grain does not lead to a degradation of the properties parallel-to-grain. Equation (17) shows the damaged compliance matrix where the single matrix entries are given.

$$C^{dam} = \begin{bmatrix} \frac{1}{(1-d_0)E_{11}} & \frac{\nu_{21}}{E_{22}} & \frac{\nu_{31}}{E_{33}} & 0 & 0 & 0 \\ \frac{\nu_{12}}{E_{11}} & \frac{1}{(1-d_{90R})E_{22}} & \frac{\nu_{32}}{E_{33}} & 0 & 0 & 0 \\ \frac{\nu_{13}}{E_{11}} & \frac{\nu_{23}}{E_{22}} & \frac{1}{(1-d_{90T})E_{33}} & 0 & 0 & 0 \\ 0 & 0 & 0 & \frac{1}{(1-d_{VR})G_{12}} & 0 & 0 \\ 0 & 0 & 0 & 0 & \frac{1}{(1-d_{VT})G_{13}} & 0 \\ 0 & 0 & 0 & 0 & 0 & \frac{1}{(1-d_{roll})G_{23}} \end{bmatrix} \quad (17)$$

In finite element programmes, the inverse of the compliance matrix C is needed in order to update the stresses. However, when calculating the inverse of the damaged compliance matrix as given in Equation (17), non-diagonal, non-zero entries of the form $\nu_{ij}(d)$ containing Poisson's ratios and damage parameters will be obtained in the damaged stiffness matrix. By means of the Poisson's ratios, the relationship between the normal stresses resp. strains is defined. Subsequently, these non-diagonal entries must also be adjusted taking damage into account: $\nu_{ij} = \nu_{ij}(d)$.

It is safe to assume that with increasing damage also the Poisson's ratios will degrade. However, except for [5], no literature is known to the author where the evolution of the Poisson's ratios during a test was measured. Linear degradation as shown in Figure 3 or exponential degradation could be implemented. Here, the chosen Poisson's ratios have the value of the damaged Poisson's ratios already at the beginning of the modelling, see Figure 3. The normal damage parameters d_0 and $d_{90R/T}$ are considered to be decoupled.

Linear degradation was implemented, but proved to be too weak in order to avoid a wrong Poisson effect which is why low Poisson's ratios from the beginning on were chosen.

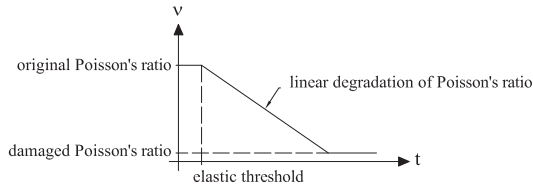


Figure 3: Degradation of Poisson's ratios

4.3 MESH REGULARISATION

Every continuum mechanics approach with softening will suffer from mesh dependency problems. The source of mesh dependency is of mathematical nature as with the onset of softening, the previously well-posed problem has turned into an ill-posed problem. In computations, this results in a stiffness matrix which is no longer positive definite. The mathematical solution is a localisation zone of zero width without energy dissipation. The numerical solution tries to capture this physically inadmissible mathematical solution which yields a localised zone of smallest possible width, i.e. a single element in most cases.

In literature, many different regularisation methods are available [e.g. 6]. Here, the crack band method as described in [7] was chosen to regularise the mesh. With the crack band method, the fracture energy is expressed in terms of characteristic finite element length h where h is a geometrical value in [length] containing information on the element's aspect ratio:

$$g_f = \frac{G_f}{h} \quad (18)$$

In equation (11), the fracture energy G_f needs to be replaced by the characteristic fracture energy g_f if the crack band model is activated. The introduction of a characteristic fracture energy g_f that is correlated to the element size provides the transformation of the fracture energy G_f into a 'mesh-dependent' value. For instance, in a coarse mesh, h will be large and leads hence to a small characteristic fracture energy g_f in comparison to the large g_f of a fine mesh with a small characteristic element length h . This adjustment of the fracture energy considering the mesh size compensates for the trend of continuum softening models to dissipate as less energy as possible.

However, the crack band model only works if one failure mode is dominating and if a localised solution occurs. It is valid if damage develops only in a band of elements and not in all elements homogeneously. Therefore, the decision whether to activate the crack band model or not must be carefully taken for each model.

Figure 4 shows load-slip graphs of a simple tension beam model where locally, slightly lower tension strength was assigned in order to trigger mesh dependency. A model with a localised softening zone was thus created and the crack band model should alleviate mesh dependency. It can be seen that the mesh dependency obtained without regularisation technique (Figure 4a) is much weaker when the crack band model is activated, see Figure 4b. [further information see 8]

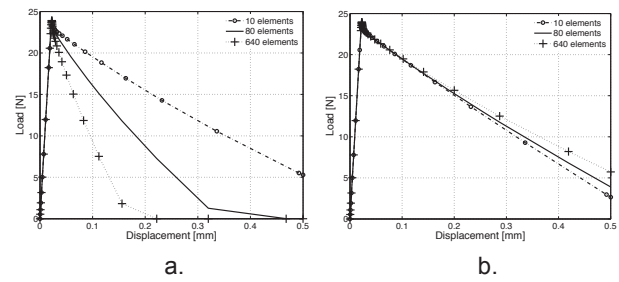


Figure 4: a. Model without regularisation, b. Crack band method activated

4.4 VISCOUS STABILISATION

Viscous stabilisation analogously to [4] is used in order to improve the convergence characteristics of the developed material model. A fictitious viscous parameter η is introduced in the model. Due to the additional viscous component, the stiffness matrix is generally positive definite. Therefore, viscous stabilisation leads to a more robust solution process with less convergence problems.

As viscosity is a time-dependent material parameter, viscous stabilisation must be a function of the rate of damage. The rate of the damage variable or of the damage threshold (= failure criteria) may be used. Equation (19) shows the stabilisation as a function of rate of damage variables:

$$\dot{d} = \frac{(d - d_v)}{\eta} \quad (19)$$

In Equation (19), the viscous parameter η defines the rate at which the true damage d and the stabilised damage d_v as defined in Equation (20) approach each other. Equation (19) can now be discretised in time. Equation (20) shows the discretised equation based on the backward Euler algorithm to insert an artificial viscosity η that is acting on the damage variables.

$$d_v^t = \max \left\{ 0, d_v^{t-1}, \frac{\eta}{\eta + dt} d_v^{t-1} + \frac{dt}{\eta + dt} d^t \right\} \quad (20)$$

As viscous stabilisation is applied to improve convergence, the energy output must be controlled in order to judge the model performance and reliability, i.e. to control that fictitious viscosity is not influencing modelling results. To this scope, the total dissipated energy and the dissipated energy associated with viscous regularisation are calculated as internal state variables. Both variables do not have any influence on the solution. They are merely used for energy output, control and post processing.

4.5 MATERIAL PROPERTIES

A major issue of all material models is the need of mechanical input parameters such as stiffness and strength values which usually derive from tests. The developed wood model needs seventeen properties as listed in Table 1 for three different wood species.

Generally, stiffness values are rather easily assembled with a satisfying reliability whereas already seemingly easy parameters as uniaxial strength values can be procured only with difficulty. This is due to two main issues. Firstly, the inherent large scatter of mechanical properties for wood and secondly, difficulties connected with testing and measuring. For instance, the uniaxial shear strength can hardly be assessed without triggering stress peaks or secondary stresses [9]. Furthermore, not always all parameters are measured, e.g. due to Poisson effect, or the positioning of the measuring instruments is not clear.

Also the fracture energies suffer from a large scatter and the fact that they are usually measured on small clear wood specimens whereas for a heterogeneous material, it can be safely assumed that fracture energies are not constant. Moreover, the needed material values are rather easily procurable for softwoods, but not for hardwoods.

In [8], a thorough literature study has been carried out where the issues around reliable material parameters are discussed and the chosen values from Table 1 are motivated.

Table 1: Material properties for spruce, beech and azobé (Variation A Beech needed for later modelling)

Para-meter	Units	Spruce (<i>Picea abies</i>)	Beech (<i>Fagus sylvatica</i>)	Azobé (<i>Lophira alata</i>)	Variation A Beech
E_{11}		11000	13000	20000	13000
$E_{22} = E_{33}$		370	860	1330	860
$G_{12} = G_{13}$		690	810	1250	810
G_{23}		50	59	91	59
$f_{t,0}$	MPa	24	41	72	41
$f_{c,0}$		36	45	58	45
$f_{t,90}$		0.7	1.0	1.0	10
$f_{c,90}$		4.3	14.2	23.2	14.2
f_v		6.9	6.9	8.6	10
f_{roll}		0.5	0.5	0.6	10
$G_{f,0}$	N/mm	60	100	180	100
$G_{f,90}$		0.5	0.71	0.71	50
$G_{f,v}$		1.2	1.2	1.5	50
$G_{f,roll}$		0.6	0.6	0.7	10
η	-	0.0001	0.0001	0.0001	0.0001

4.6 SUMMARY

The developed material model was programmed in a user subroutine UMAT and inserted into the commercial FE software ABAQUS®.

Figure 5 shows the flow diagram of the developed CDM material subroutine. The subroutine is given in [10].

The introduced material model based on piecewise defined failure criteria and several damage parameters following elastic perfectly plastic or linear softening laws represents a simplified approach for wood.

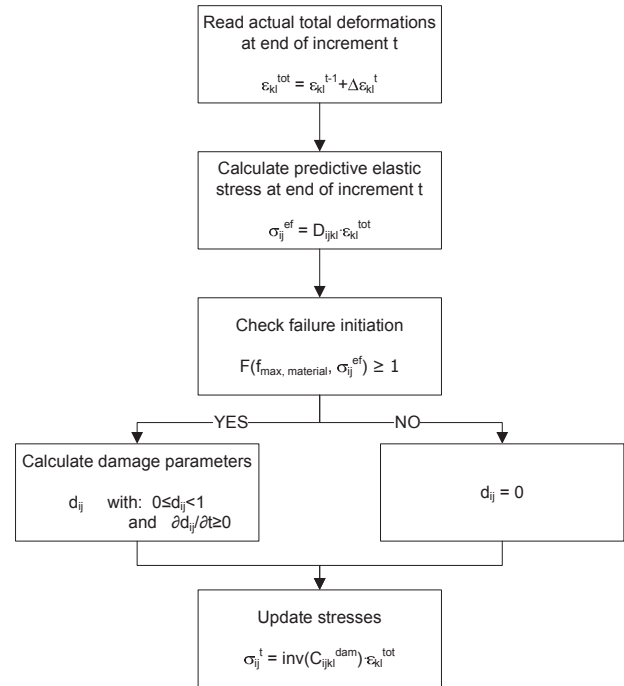


Figure 5: Flow diagram of CDM

Densification, fibre kinking or other effects due to the anatomical structure cannot be modelled. However, after a thorough literature study of both available modelling approaches and mechanical material behaviour [8], the innovative potential of CDM in combination with clear and simple constitutive laws is convincing.

Simple constitutive laws with explicit mechanical properties facilitate understanding and inspection of the models. No smeared input values need to be introduced and their effect can be directly translated to the model results.

The chosen CDM approach allows for identification of failure modes and visualisation of damage. For instance, progressive damage during a loading process is easily visualised in the post processing. Ductile and brittle failure modes can be combined in a holistic 3D material model and mixed failures combining ductile and brittle modes occurring for instance under loading with an angle to the grain can be captured. Also early damage in e.g. embedment tests due to transverse or shear stress components can be captured while the global load-slip behaviour of the model is still ductile.

5 MODELLING

5.1 VALIDATION

When developing constitutive laws, results of single element models or on models with few elements need to be validated. For this purpose, different model validations were carried out among which compression on a cube with different angles to the grain.

Figure 6 shows modelling results on spruce wood using the developed UMAT together with the FE model (here with 125 linear brick elements with full integration). The crack band model was deactivated as no local crack band is expected and therefore, the crack band model is not

valid. As can be observed in Figure 6, compression parallel- and perpendicular-to-grain showed elastic perfectly plastic behaviour as implemented whereas for 22.5° and 45°, brittle behaviour due to the influence of brittle shear damage laws could be observed. This can be confirmed with test results, see [5], [8].

Figure 7 shows the overlap of the Hankinson equation [11] with FE results (same model as shown in Figure 6, but consisting of one element). The load carrying capacity can be satisfyingly predicted with a maximum difference between FE model and Hankinson equation of 15%.

Figure 6 and Figure 7 underline the prediction capability of the CDM model. Not only load carrying capacities can be predicted, but also the general stress-strain behaviour with combined ductile and brittle failures. Especially the prediction of the different load-slip behaviour between the models loaded at an angle to the grain of 22.5°, brittle, and 45°, more ductile, is good. Further validations were carried out with different mesh size and material orientations, different loading from reversed cyclic loading to combined loading of normal stresses and shear. All validations are shown in [5] and confirmed the correct implementation and calculation of the subroutine.

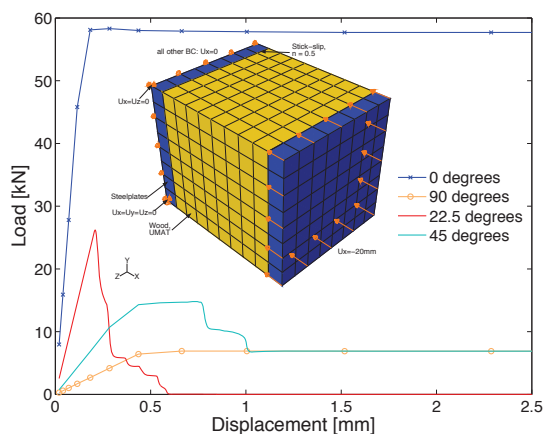


Figure 6: Results FE model for compression with different angles to the grain, spruce

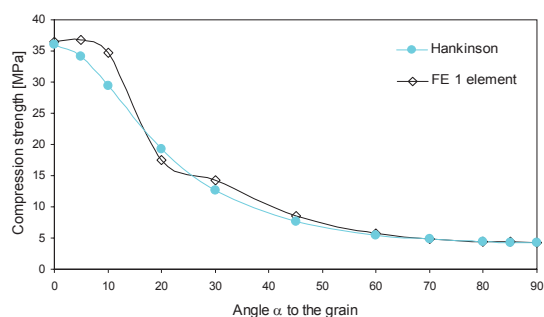


Figure 7: Superposition of FE results with Hankinson equation, spruce

5.2 MATERIAL MODELS

In order to verify the capability of the models to predict the mechanical behaviour of wood, available material tests from literature were modelled. Material tests do not

yet contain any other material laws or contact formulations and are the first logical modelling step before developing embedment models.

The chosen tests were undertaken by [5]. Tension tests parallel-to-grain as shown in Figure 8 with asymmetric dog bone specimens with a tapered area of 2 x 20 mm are presented here. For other material tests, please refer to [8]. All tests were carried out on small clear spruce specimens. However, the material parameters for spruce used in the FE models were derived for structural-size wood and are given in Table 1. Linear bricks with full integration were used and the crack band model was activated.

Figure 9 shows the modelling results in terms of load-slip where some increments are indicated. The same increments are shown in Figure 10 in terms of damage variable $d_{t,0}$ for damage due to tension parallel-to-grain. The crack development in the tapered area (which is asymmetric due to the specimen geometry) is clearly identified. Furthermore, stable crack growth can be modelled.

The comparison with three typical lower bound test results [5] showed good qualitative agreement. However, the load carrying capacity was generally underestimated which is explicable as the chosen material properties for modelling were based on structural-size wood whereas the tests were on clear wood.

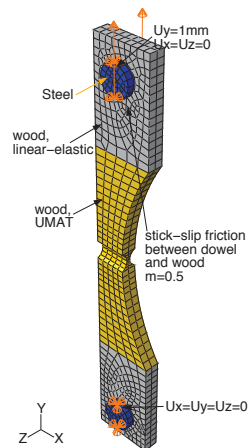


Figure 8: Tension parallel-to-grain, geometry from [5]

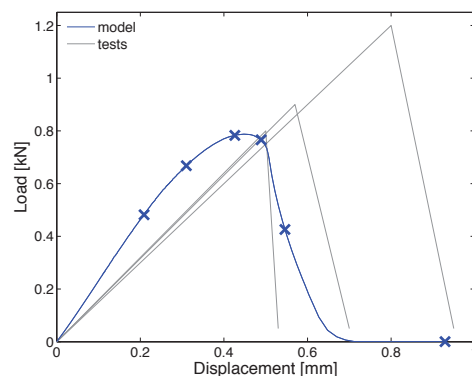


Figure 9: Load-slip graph of tension model

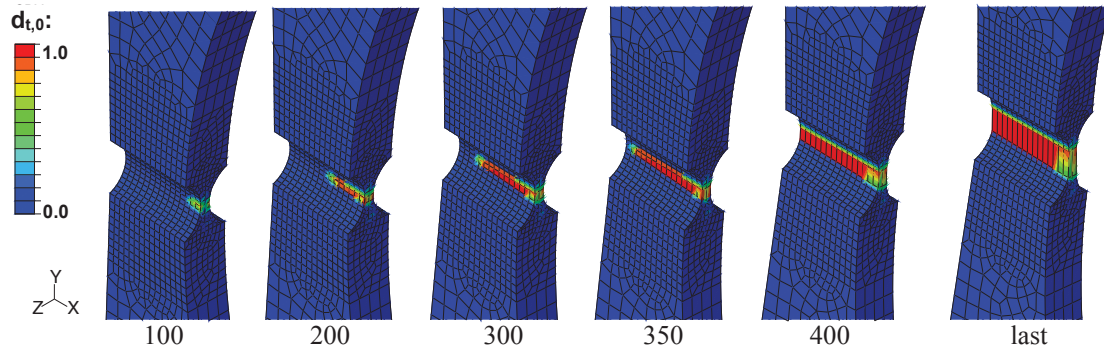


Figure 10: Tension parallel-to-grain, damage variable $d_{t,0}$ at indicated increments

5.3 EMBEDMENT MODELS

Embedment models were developed whose outcomes could be verified with tests taken from literature [12]. Three different wood species were chosen, spruce, beech and azobé. The material properties are given in Table 1. The FE model is shown in Figure 11, only a quarter of an embedment specimen with a 24 mm dowel was modelled. Also here, no localised damage is expected and the crack band model was deactivated. Again, 3D solids with linear interpolation between the eight integration points were chosen. Friction between dowel and wood was simulated with the stick-slip model and a friction coefficient of $\mu = 0.5$.

Figure 12 shows exemplarily the modelling outcomes of embedment models in comparison with test results. In Figure 12, damage due to compression parallel-to-grain directly underneath the dowel of a spruce specimen can be clearly seen. Also brittle damage due to tension perpendicular-to-grain and shear is identified. Both failure modes are coupled as defined in Equation (4). Furthermore, two elements are indicated in Figure 12 whose integration point results in terms of tension perpendicular-to-grain and longitudinal shear are given in Figure 13. It can be seen that damage in element a initiated due to high shear stresses and in element b, damage was triggered by high tension stresses perpendicular-to-grain. Both predictions are correct if the position of the elements in the model is considered.

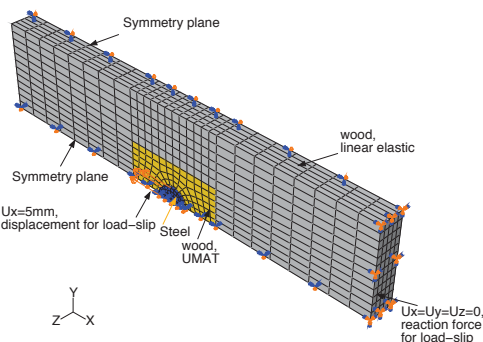


Figure 11: Quarter of embedment model with boundary conditions, materials and default mesh

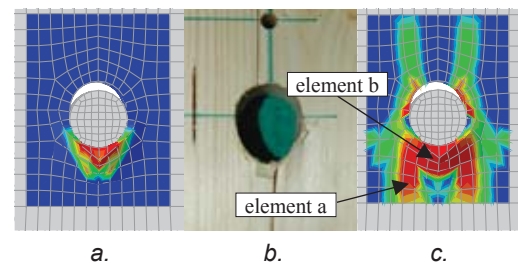


Figure 12: Embedment of spruce with 24mm dowel, a. damage variable $d_{c,0}$ in compression parallel-to-grain, b. test result, c. damage variable $d_{t,90}$ in tension perpendicular-to-grain

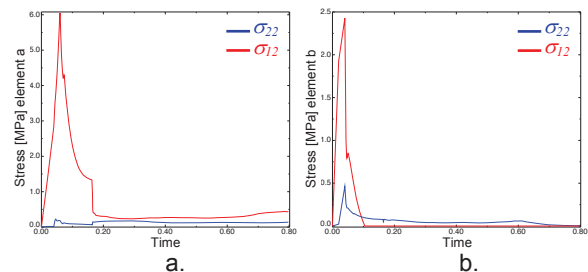


Figure 13: Stress components σ_{22} and σ_{12} ; a. element a; b. element b (Figure 12)

Figure 14 shows load-slip graphs of azobé specimens in overlap with the modelling result. The stiffness prediction is good. The reached displacement was too low. However, the source of the brittle failure mode observed in Figure 14 is purely numerical and is not expressing the splitting of the embedment model. Once the row of elements directly underneath the dowel fails, spurious energy modes develop. Basically, the model fails completely on a local level of collapsed elements whereas the neighbouring elements still can carry load. To clarify these spurious energy modes, Figure 15 shows typical strain evolution for an element of the tension test parallel-to-grain (Figure 8). It can be observed that once the element collapses in 3D, high values in all strain components develop. The global load shows a sudden drop and calculation exits. Thereby, the model shows numerical softening due to these local failures and no complete physical damage.

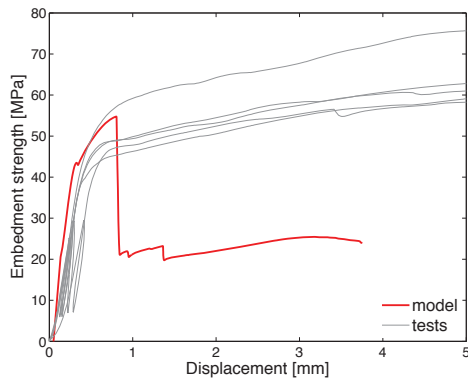


Figure 14: FE result versus test results of embedment tests on azobé with 24mm dowels

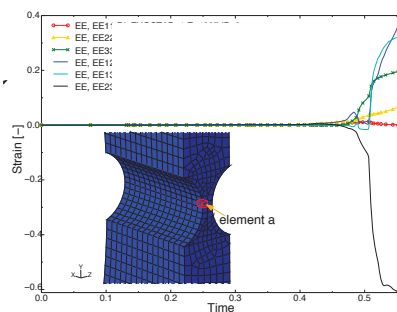


Figure 15: Typical strain components of indicated element a, model shown in Figure 6

Accordingly, there are three main options to improve the model performance and to avoid local early brittle failures due to spurious energy modes:

- Introduction of a threshold value for the damage variables in order to avoid complete damage and to keep a residual stiffness. This however is not thought to be a good solution as an uncontrollable fictitious parameter would be introduced.
- Change resp. increase mechanical properties in order to avoid early complete damage of elements.
- Reformulate and smear damage over more than one element, disassociate damage from the single integration points.

Point three is part of future research as then, the material subroutine will be optimised and solutions will be developed to control excessive element distortion.

The second option however was carried out in order to understand the influence of the material parameters. Also considering the rather difficult determination of material properties, it is thought to be admissible to modify these parameters. Table 1 gives modified material parameters for beech wood nominated “variation A” where the properties defining the 3D brittle behaviour are increased. Figure 16 shows the modelling results for an embedment test specimen with the default properties for beech and variation A superposed with test results. The load-slip behaviour applying the default properties shows again too brittle behaviour due to numerical softening. The model using modified properties “variation A” reaches higher deformations before failure. The higher values for strength and fracture energies as

defined for “variation A” lead to numerical softening at higher deformations which is more realistic.

As the resulting curve for “variation A” still yields too high strength values, also the compression strength parallel-to-grain is reduced as indicated in Figure 16. Such a reduction is thought to reduce the load carrying capacity and should therefore lead to a lower plateau.

Modelling outcomes confirmed this. A better overlap between tests and model can thus be obtained purely by modifying clearly recognisable mechanical properties.

Another important outcome of modelling can also be deduced from Figure 16. The earlier initiation of damage in the default model with a decrease in stiffness in comparison to “variation A” is clearly observable in the detail. The global stiffness is thus decreasing although the model still shows a very clear load increase. This is a realistic prediction.

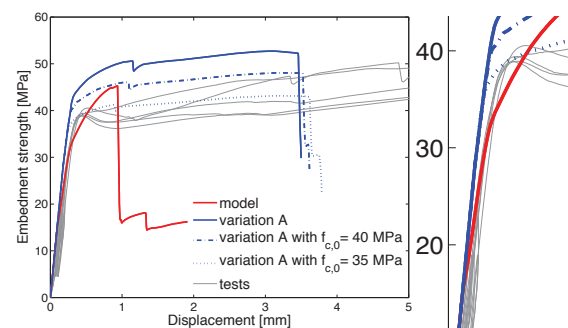


Figure 16: FE result versus test results of embedment tests on beech with 24mm dowels, material parameters modified – variation A, with detail

6 CONCLUSIONS

A promising holistic constitutive 3D model for the material wood could be developed that can identify failure modes and combine simultaneous ductile and brittle failures within one model. The mechanical material parameters needed for the constitutive relationship are clearly defined. The material model runs in a complex FE environment in combination with other material models and contact formulations.

The developed material model is a simplified material model that cannot perfectly reproduce material tests, e.g. kink bands or densification cannot be represented. It could be shown however that such a simplified model is sufficiently precise for more complex models than pure material models, i.e. embedment models.

First modelling results were satisfying in terms of stiffness and load carrying capacity. Numerical softening caused by spurious energy modes of completely collapsed elements however led to early brittle failure of models that did not represent physical failure. Furthermore, once unloading has started in the most stressed elements, the load is not transferred to neighbouring elements. These numerical problems need to be solved in order to optimise the subroutine.

As for any other modelling approach, a major issue lies in the determination of the needed mechanical properties. As the model performance and prediction

capacity is highly dependent on these properties, methods to derive reliable values must be developed.

REFERENCES

- [1] Hill R. A theory of the yielding and plastic flow of anisotropic metals. *Proceedings Royal Society (London), Series A*, 193, 281-297, 1948.
- [2] Hoffman, O. The brittle strength of orthotropic materials. *Journal of Composite Materials*, 1, 200-206, 1967.
- [3] Maimí, P. Modelización constitutiva y computacional del daño y la fractura de materiales compuestos. *PhD thesis*, Universitat de Girona, 2006.
- [4] Matzenmiller, A., Lubliner, J. and Taylor, R.L. A Constitutive Model for Anisotropic Damage in Fiber-Composites. *Mechanics of Materials*, 20, 125-152, 1995.
- [5] Franke, S. Zur Beschreibung des Tragverhaltens von Holz unter Verwendung eines photogrammetrischen Messsystems. *PhD thesis*, Bauhaus-Universität Weimar, 2008.
- [6] Sluys, L.J. Wave Propagation, Localisation and Dispersion in Softening Solids. *PhD thesis*, Technische Universiteit Delft, 1992.
- [7] Bažant, Z.P. and Oh, B.H. Crack band theory for fracture of concrete. *Matériaux et Constructions*, 16, 155-177, 1983.
- [8] Sandhaas, C. Mechanical behaviour of timber joints with slotted-in steel plates. *PhD thesis*, University of Technology Delft, in preparation.
- [9] Moses, D.M. and Prion, H.G.L. Stress and failure analysis of wood composites: a new model. *Composites Part B-Engineering*, 35, 251-261, 2004.
- [10] Sandhaas, C. 3D Material Model for Wood, Based on Continuum Damage Mechanics. *Stevinrapport 6-11-4*, Stevin II Laboratory, University of Technology Delft, 2011.
- [11] Hankinson, R.L. Investigation of crushing strength of spruce at varying angles of grain. *U. S. Air Service Information Circular* Vol. 3 No. 259, 1921.
- [12] Sandhaas C., van de Kuilen J.W., Blass H.J. and Ravenshorst G. Embedment tests parallel-to-grain and ductility in tropical hardwood species. *Proceedings WCTE*. Riva del Garda, Italy, 2010.

Finite Element Software package:

ABAQUS® Version 6.8, Dassault Systèmes Simulia Corp., Providence, RI, USA, 2008.